Precise Determination of the Strong Coupling Constant
from Dijet Cross Sections up to the Multi-TeV Range

Fazila Ahmadova,[1, 2] Daniel Britzger,[1] Xuan Chen,[3] Johannes Gäßler,[4] Aude Gehrmann–De Ridder,[5, 2]
Thomas Gehrmann,[2] Nigel Glover,[6] Claire Gwenlan,[7] Gudrun Heinrich,[8]
Alexander Huss,[9] Lucas Kunz,[8] João Pires,[10, 11] Klaus Rabbertz,[4] and Mark Sutton[12]

[1] *Max-Planck-Institut für Physik, Boltzmannstr. 8, 85748 Garching, Germany*
[2] *Department of Physics, Universität Zürich, Winterthurerstrasse 190, CH-8057 Zürich, Switzerland*
[3] *School of Physics, Shandong University, Jinan, Shandong 250100, China*
[4] *Karlsruhe Institute of Technology (KIT), Institute for Experimental Particle Physics,*
Wolfgang-Gaede-Str. 1, 76131 Karlsruhe, Germany
[5] *Institute for Theoretical Physics, ETH, Wolfgang-Pauli-Strasse 27, CH-8093 Zürich, Switzerland*
[6] *Institute for Particle Physics Phenomenology, University of Durham, Durham, DH1 3LE, United Kingdom*
[7] *Department of Physics, The University of Oxford, Oxford, OX1 3PU, United Kingdom*
[8] *Karlsruhe Institute of Technology (KIT), Institute for Theoretical Physics,*
Wolfgang-Gaede-Str. 1, 76131 Karlsruhe, Germany
[9] *Theoretical Physics Department, CERN, CH-1211 Geneva 23, Switzerland*
[10] *LIP, Avenida Professor Gama Pinto 2, P-1649-003 Lisboa, Portugal*
[11] *Faculdade de Ciências, Universidade de Lisboa, 1749-016 Lisboa, Portugal*
[12] *Department of Physics and Astronomy, The University of Sussex, Brighton, BN1 9RH, United Kingdom*
(Dated: December 30, 2024)

We determine the value of the strong coupling α_s and study its running over a wide range of scales as probed by the dijet production process at hadron colliders, based on an NNLO QCD analysis of LHC dijet data. From a large subset of these data a value of $\alpha_s(m_Z) = 0.1178 \pm 0.0022$ is obtained for the strong coupling at the scale of the Z-boson mass m_Z, using the invariant mass of the dijet system to select the scale where α_s is probed. The combination of different data sets enhances the reach and precision of the analysis in the mutli-TeV range and allows for the first determination of α_s up to scales of 7 TeV. Complementing the LHC data with dijet cross sections measured at the HERA electron–proton collider, the kinematic range is extended to test the running of the strong coupling towards smaller scales. Our results exhibit excellent agreement with predictions based on the renormalization group equation of QCD, and represent a comprehensive test of the asymptotic behavior of QCD, spanning more than three orders of magnitude in energy scale.

I. Introduction The theory of Quantum Chromodynamics (QCD) [1–5] so far successfully describes the dynamics and asymptotic behavior of the strong interaction. The renormalization group equation (RGE) of QCD predicts the scale evolution ("running") of its coupling α_s. Consequently, the determination of the strong coupling at different energy scales probes the non-Abelian gauge structure of QCD. Despite its outstanding importance as the only free parameter of massless QCD, the value of the strong coupling constant at the reference scale of the Z-boson mass, $\alpha_s(m_Z)$ is known with an uncertainty of approximately 1 % [6] and hence is one of the least precisely determined fundamental constants in physics.

In this letter we make use of new precise predictions from perturbative QCD (pQCD) for dijet production at next-to-next-to leading order (NNLO) including subleading color contributions [7–9] to determine the value of the strong coupling constant $\alpha_s(m_Z)$. We use precise dijet production data recorded by the ATLAS [10, 11] and CMS [12–14] experiments in proton–proton collisions (pp) at the LHC at center-of-mass energies of 7, 8, and 13 TeV. The analysis is further extended to include dijet cross sections measured in electron–proton (ep) collisions at the HERA collider [15–19], which operated at consid-

erably lower center-of-mass energies of $\sqrt{s} = 300$ and 320 GeV. This allows the investigation of the running of the strong coupling $\alpha_s(\mu_R)$ over energy scales ranging from a few GeV to the TeV regime. The first theoretical studies of dijet production were performed at next-to-leading order (NLO) in pQCD in Refs [20, 21]. The first applications of NNLO predictions to determine α_s were carried out using e^+e^- event shape data in Ref. [22] and using DIS jet production in Ref. [23]. Recent determinations of α_s in pp collisions were performed at NNLO in a leading-color approximation with inclusive jet and dijet cross sections [14, 24–26], and with multijet transverse energy correlations based on 3-jet NNLO predictions [27–29]. Extending to 4.2 TeV, these predictions allow the measurement of α_s at the largest scales attained up till now. By using multiple dijet data sets, our analysis achieves a considerably higher reach and resolution above scales of one TeV, allowing a measurement of α_s with unprecedented precision in the range beyond 1 TeV, extending as far as 7 TeV.

II. Methodology The value of $\alpha_s(\mu_R)$ is determined by performing a least-squares minimization of the complete NNLO pQCD predictions for selected inclusive dijet cross-sections from the ATLAS and CMS experiments at pp center-of-mass energies $\sqrt{s}$ of 7, 8, and

13 TeV, summarized in Table I. Two measurements from

Data	$\sqrt{s}$ [TeV]	$\mathrm{d}\sigma$	R	$\mathcal{L}$
ATLAS [10]	7	$\frac{\mathrm{d}^2\sigma}{\mathrm{d}m_{\mathrm{jj}}\mathrm{d}y^*}$	0.6	$4.5\,\mathrm{fb}^{-1} \pm 1.8\,\%$
CMS [12]	7	$\frac{\mathrm{d}^2\sigma}{\mathrm{d}m_{\mathrm{jj}}\mathrm{d}y_{\mathrm{max}}}$	0.7	$5.0\,\mathrm{fb}^{-1} \pm 2.2\,\%$
CMS [13]	8	$\frac{\mathrm{d}^3\sigma}{\mathrm{d}\langle p_{\mathrm{T}}\rangle_{1,2}\mathrm{d}y^*\mathrm{d}y_{\mathrm{b}}}$	0.7	$19.7\,\mathrm{fb}^{-1} \pm 2.6\,\%$
ATLAS [11]	13	$\frac{\mathrm{d}^2\sigma}{\mathrm{d}m_{\mathrm{jj}}\mathrm{d}y^*}$	0.4	$3.2\,\mathrm{fb}^{-1} \pm 2.1\,\%$
CMS [14]	13	$\frac{\mathrm{d}^2\sigma}{\mathrm{d}m_{\mathrm{jj}}\mathrm{d}y_{\mathrm{max}}}$	0.8	$33.5\,\mathrm{fb}^{-1} \pm 1.2\,\%$
CMS [14]	13	$\frac{\mathrm{d}^3\sigma}{\mathrm{d}m_{\mathrm{jj}}\mathrm{d}y^*\mathrm{d}y_{\mathrm{b}}}$	0.8	$29.6\,\mathrm{fb}^{-1} \pm 1.2\,\%$

TABLE I. Selected dijet data sets with center-of-mass energy $\sqrt{s}$, cross-section definition $d\sigma$, jet size parameter R and integrated luminosity $\mathcal{L}$.

ATLAS at $\sqrt{s} = 7$ and $13\,\mathrm{TeV}$ are available as functions of the dijet mass $m_{\mathrm{jj}} = \sqrt{(p_{j_1} + p_{j_2})^2}$, and half of the absolute rapidity separation $y^* = |y_1 - y_2|/2$, where p_{j_1}, p_{j_2} and y_1, y_2 denote the four-momenta and rapidities, respectively, of the two jets leading in p_{T}. Double-differential measurements have been performed by CMS at $\sqrt{s} = 7$ and $13\,\mathrm{TeV}$, as functions of m_{jj} and the maximum absolute rapidity, y_{max}, of either of the two leading p_{T} jets. CMS has also published triple-differential cross sections at $\sqrt{s} = 8$ and $13\,\mathrm{TeV}$ as functions of either m_{jj} or the average transverse momentum of the two leading jets, $\langle p_{\mathrm{T}}\rangle_{1,2}$, half of their rapidity separation y^*, and the longitudinal boost of the dijet system given by $y_{\mathrm{b}} = |y_1 + y_2|/2$. These measurements employ the anti-k_{t} jet algorithm [30], but use different jet size parameters R. When cross sections are provided for more than one value of R, the larger jet size parameter is selected due to the expected improved perturbative convergence [31]. The CMS $13\,\mathrm{TeV}$ data are provided in both double- and triple-differential forms, but only one of the two data sets can be considered in the combined study because of their experimental correlations. We choose the double-differential variant in the following due to its larger range in m_{jj}. In order to reduce the sensitivity to parton distribution functions (PDFs), the selected data are restricted to $y^* < 2.0$ (respectively $y_{\mathrm{max}} < 2.0$) and $y_{\mathrm{b}} < 1.0$. The selected data then have further experimental advantages since in the selected regions the tracking detectors of the experiments can be used. Finally, altogether 367 out of 493 cross section measurements are considered in the α_{s} determination.

The dijet data are confronted with predictions in the framework of pQCD at NNLO [32, 33] as implemented in the NNLOJET framework [34, 35]. The α_{s} sensitivity in this calculation arises from two components: the hard matrix elements and the PDFs. The NNLO predictions include the full set of contributions, in particular all sub-leading color parts [7–9], which are, for the first time, used in the determination of α_{s} with LHC jet data. Using the APPLfast library [24, 36], the NNLO pQCD coefficients are stored independently of the $\alpha_{\mathrm{s}}(m_{\mathrm{Z}})$ value and PDF. The statistical uncertainty, derived from the Monte Carlo integration in NNLOJET, is typically around a percent or below. The momentum distribution of partons inside the incoming proton is obtained from PDFs. The x-dependence of the PDFs is defined at a starting scale μ_0, and the PDFs are evolved to the factorization scale μ_{F} using DGLAP evolution, with α_{s} as a free parameter, where they are convolved with the hard coefficients. We set the scale μ_0 to $90\,\mathrm{GeV}$, a characteristic hard scale, and the x-dependence is taken from the PDF4LHC21 PDF combination [37]. The predictions further include bin-wise correction factors for non-perturbative effects (NP) and higher-order electroweak (EW) contributions [38]. Both correction factors and their uncertainties are taken as published by the experimental collaborations [10–14]. Further details on the evaluation of the theory predictions are collected in Appendix A. A comprehensive study to assess the agreement between the NNLO pQCD predictions and the dijet data, as well as the consistency of individual data sets across different kinematic regions and between multiple data sets is provided in Ref. [39]. Overall, good agreement is observed between the predictions and the data in all kinematic regions and for all data sets, with a very good consistency between the data sets.

The value of $\alpha_{\mathrm{s}}(m_{\mathrm{Z}})$ is then determined through a least-squares fit of the NNLO predictions to the dijet data, similar to the method used in Refs. [23, 40]. The uncertainties considered in the fit include experimental, non-perturbative (NP), NNLO statistical, and PDF uncertainties. Their covariance matrices also take correlations between data points and data sets into account. Henceforth, the linearly propagated uncertainty from that fit will be denoted as "(fit,PDF)" uncertainty to emphasize that this uncertainty comprises experimental and PDF related uncertainties together. Details on the χ^2 minimization and considerations on the PDF uncertainties are discussed in Appendix B.

Further uncertainties due to additional uncertainties in the predictions are derived as follows. The starting scale of the PDF evolution, μ_0, can be arbitrarily chosen, and is thus associated with an uncertainty. We repeat the fit with μ_0 varied by factors of 0.5 or 2 and report half of the difference between these two fit results as an uncertainty (denoted as "(μ_0)" or PDFμ_0). In addition, also the value of $\alpha_{\mathrm{s}}(m_{\mathrm{Z}})$ as used in the PDF determination needs to be considered to be uncertain. However, such an uncertainty in the PDFs is already equivalently represented through the variation of the starting scale μ_0 and therefore is not considered separately. Dedicated fits with PDFs that were determined with different values of $\alpha_{\mathrm{s}}(m_{\mathrm{Z}})$ support this statement and we observe that the PDFμ_0 uncertainty corresponds approximately to a variation of ± 0.001 of $\alpha_{\mathrm{s}}(m_{\mathrm{Z}})$ in the PDF set.

An additional scale uncertainty accounts for missing higher orders beyond NNLO and for the actual choice of the renormalization μ_{R} and factorization μ_{F} scales. It is derived by varying μ_{R} and μ_{F} independently by factors of 0.5, 1, or 2 around the central value $\mu_{\mathrm{R}} = \mu_{\mathrm{F}} = m_{\mathrm{jj}}$ in

the complete NNLO pQCD predictions, omitting the two variations of $(0.5, 2)$ and $(2, 0.5)$, i.e. using the so-called 7-point scale variations. Half of the difference between the largest and smallest prediction is reported as *scale* uncertainty (denoted as "$(\mu_{\mathrm{R}},\mu_{\mathrm{F}})$"), since the asymmetry in these variations is typically small.

III. Results from LHC dijets The value of the strong coupling at the scale m_{Z} [6] is determined from the five LHC dijet data sets using complete NNLO pQCD predictions. The fit exhibits an excellent consistency with $\chi^2/n_{\mathrm{dof}} = 0.92$ and the value of $\alpha_{\mathrm{s}}(m_{\mathrm{Z}})$ is determined to be

$$\alpha_{\mathrm{s}}(m_{\mathrm{Z}}) = 0.1178 \, (14)_{\mathrm{(fit,PDF)}} \, (1)_{(\mu_0)} \, (17)_{(\mu_{\mathrm{R}},\mu_{\mathrm{F}})} \, .$$

Fits of $\alpha_{\mathrm{s}}(m_{\mathrm{Z}})$ were also performed for individual data sets. The results are collected in Table II and displayed in Fig. 1, where they are compared to the combined fit from all five data sets and to the world average value [6].
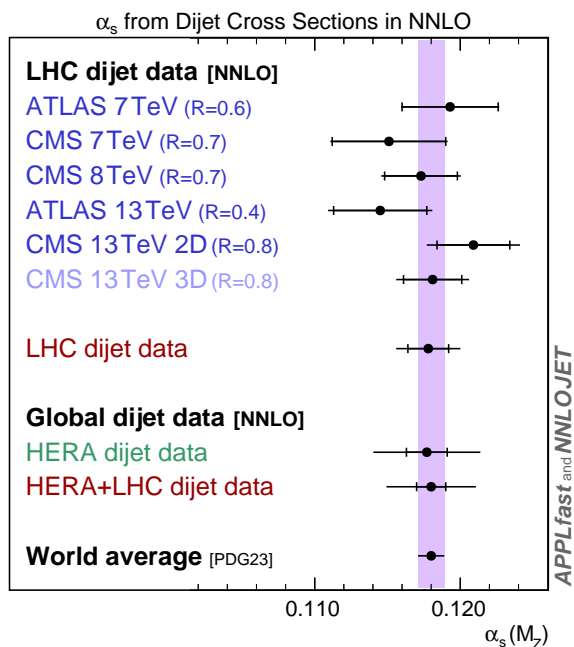

FIG. 1. Comparison of $\alpha_{\mathrm{s}}(m_{\mathrm{Z}})$ determinations from dijet cross sections to the world average value. The inner error bars indicate the (fit,PDF) uncertainty, and the outer error bars further include the scale and μ_0 uncertainty.

The results from the individual data sets exhibit (fit,PDF) uncertainties in the range between ± 0.0020 to ± 0.0039. Data sets with larger integrated luminosity or at higher center-of-mass energy yield smaller uncertainties. The $\alpha_{\mathrm{s}}(m_{\mathrm{Z}})$ values are consistent with the world average value. It is observed that the determination of $\alpha_{\mathrm{s}}(m_{\mathrm{Z}})$ using all five LHC dijet data sets benefits significantly from independent measurements, extended kinematic ranges, and multiple center-of-mass energies. Hence, the experimental uncertainties are found to be reduced in the combined determination in comparison to

Data set	χ^2/n_{dof}	$\alpha_{\mathrm{s}}(m_{\mathrm{Z}})$
ATLAS 7 TeV	74.7/ 77	0.1193 (33) (4) (6)
ATLAS 13 TeV	87.7/106	0.1145 (32) (4) (16)
CMS 7 TeV	50.7/ 45	0.1151 (39) (1) (9)
CMS 8 TeV	37.0/ 56	0.1173 (25) (0) (11)
CMS 13 TeV (2D)	71.6/ 78	0.1209 (25) (2) (20)
CMS 13 TeV (3D)	137.7/112	0.1181 (20) (1) (15)
LHC dijets (CMS13-2D)	335.3/366	0.1178 (14) (0) (17)
LHC dijets (CMS13-3D)	397.9/400	0.1172 (14) (0) (14)
HERA	92.8/118	0.1177 (14) (1) (34)
LHC+HERA (CMS13-2D)	428.4/485	0.1180 (10) (0) (29)
LHC+HERA (CMS13-3D)	491.0/519	0.1177 (10) (0) (27)

TABLE II. Results of $\alpha_{\mathrm{s}}(m_{\mathrm{Z}})$ from fits of complete NNLO pQCD predictions to dijet cross section data. Listed are the values of $\alpha_{\mathrm{s}}(m_{\mathrm{Z}})$ with the (fit,PDF) uncertainty, the (μ_0) uncertainty, and the scale uncertainty $(\mu_{\mathrm{R}},\mu_{\mathrm{F}})$. The upper rows display results from fits to individual data sets. The middle rows show results from fits to all studied LHC dijet data; once using the double-differential (2D) or triple-differential (3D) CMS 13 TeV data. The bottom rows show results from fits to HERA dijet data and from fits to LHC and HERA dijet data taken together.

any individual data set. An additional variant of the nominal fit using the CMS 3D data is presented in appendix C.

IV. Including HERA dijet data The analysis is extended by further including data for dijet production in neutral-current deep-inelastic scattering (NC DIS) taken at the HERA ep collider. These data, from the H1 [15, 16, 18, 19] and ZEUS [17] collaborations, have previously been used for α_{s} determinations at NNLO accuracy [23, 41, 42] using the complete NNLO pQCD predictions [40, 43, 44]. Further details on the data are collected in Appendix D and the results of a fit to the HERA dijet measurements alone is presented in Table II. Using the HERA data provides competitive (fit,PDF) uncertainties in $\alpha_{\mathrm{s}}(m_{\mathrm{Z}})$, but the fit exhibits sizable scale uncertainties.

In the combined fit to HERA plus LHC data, altogether 612 dijet cross section data values are available. After applying the y^*, y_{b} and y_{max} data selection criteria, 486 data points remain for the combined fit, which yields

$$\alpha_{\mathrm{s}}(m_{\mathrm{Z}}) = 0.1180 \, (10)_{\mathrm{(fit,PDF)}} \, (0)_{(\mu_0)} \, (29)_{(\mu_{\mathrm{R}},\mu_{\mathrm{F}})}$$

with $\chi^2/n_{\mathrm{dof}} = 0.88$. The χ^2 value suggests an excellent consistency between the HERA and LHC data, as well as an outstanding agreement between data and the NNLO pQCD predictions. The α_{s} value is found to be in excellent agreement with the world average value of $\alpha_{\mathrm{s}}(m_{\mathrm{Z}})$ of 0.1180 (10) [6]. As expected, the experimental uncertainties are reduced in the combined fit as compared to the fits to HERA or LHC data alone. However, the scale uncertainty is found to be the dominant uncertainty and

$\mu_{\mathrm{R}}^{\mathrm{avg}}$ [GeV]	$\alpha_{\mathrm{s}}(m_{\mathrm{Z}})$	$\alpha_{\mathrm{s}}(\mu_{\mathrm{R}})$
7.4	0.1214 (28) (1) (69)	0.2013 (82) (4) (205)
10.1	0.1207 (15) (1) (56)	0.1840 (37) (2) (138)
13.3	0.1171 (15) (0) (41)	0.1654 (31) (0) (84)
17.2	0.1151 (20) (0) (29)	0.1530 (36) (1) (53)
20.1	0.1160 (20) (1) (31)	0.1498 (34) (1) (52)
24.5	0.1159 (18) (0) (27)	0.1442 (29) (1) (43)
29.3	0.1175 (23) (0) (24)	0.1418 (33) (0) (35)
36.0	0.1171 (26) (0) (25)	0.1362 (35) (1) (34)
49.0	0.1157 (26) (1) (17)	0.1275 (31) (1) (20)
77.5	0.1105 (37) (3) (8)	0.1131 (39) (3) (8)
250	0.1180 (15) (1) (14)	0.1025 (11) (1) (11)
370	0.1181 (15) (1) (16)	0.0975 (10) (1) (11)
550	0.1174 (15) (1) (19)	0.0925 (9) (1) (12)
810	0.1173 (15) (2) (20)	0.0885 (9) (1) (11)
1175	0.1171 (16) (2) (22)	0.0848 (8) (1) (11)
1760	0.1171 (17) (2) (24)	0.0813 (8) (1) (11)
2545	0.1171 (18) (2) (26)	0.0783 (8) (1) (12)
3490	0.1171 (20) (2) (28)	0.0760 (8) (1) (12)
4880	0.1185 (31) (3) (34)	0.0742 (12) (1) (13)
7040	0.1232 (128) (12) (37)	0.0734 (43) (4) (13)

TABLE III. Results for the running of the strong coupling. The values are reported for different μ_{R} intervals. The columns show the central μ_{R} value, the resulting value of $\alpha_{\mathrm{s}}(m_{\mathrm{Z}})$, and the corresponding value of $\alpha_{\mathrm{s}}(\mu_{\mathrm{R}})$. The brackets denote the (fit,PDF), the (μ_0) and the ($\mu_{\mathrm{R}}, \mu_{\mathrm{F}}$) uncertainty.

is significantly larger than in the fit to LHC data alone. This is due to the HERA data, which reside at lower energy scales and thus exhibit larger scale uncertainties. The scale variations of the dijet predictions for the *ep* and *pp* cross sections are considered to be fully correlated, both between the data sets and across the entire phase space. It may be interesting to study these correlations more extensively to allow the dominant scale uncertainty to be reduced. Such a study is however, beyond the scope of this work.

V. Running of the strong coupling The asymptotic behavior of the strong coupling is one of the key properties of QCD [2–4]. Its prediction needs to be validated with experimental data, for example by probing the running of $\alpha_{\mathrm{s}}(\mu_{\mathrm{R}})$ by determining α_{s} at different values of μ_{R}. For such a study, dijet cross sections represent a particularly powerful opportunity, since the dijet system provides a natural choice for the renormalization scale μ_{R}, which in principle could be chosen freely. As before, for dijet production in *pp* collisions μ_{R} is identified with m_{jj}, while for *ep* data $\mu_{\mathrm{R}}^2 = Q^2 + \langle p_{\mathrm{T}} \rangle_{1,2}^2$ [23] is used. The μ_{R} values of the HERA and LHC dijet cross sections span over three orders of magnitude from about 7 GeV up to 7 TeV.

Each cross section measurement is then assigned a single representative value of μ_{R}. These values are used (only) to group the data into 20 distinct μ_{R} intervals. It is confirmed that in each μ_{R} interval, data from multiple data sets are considered.
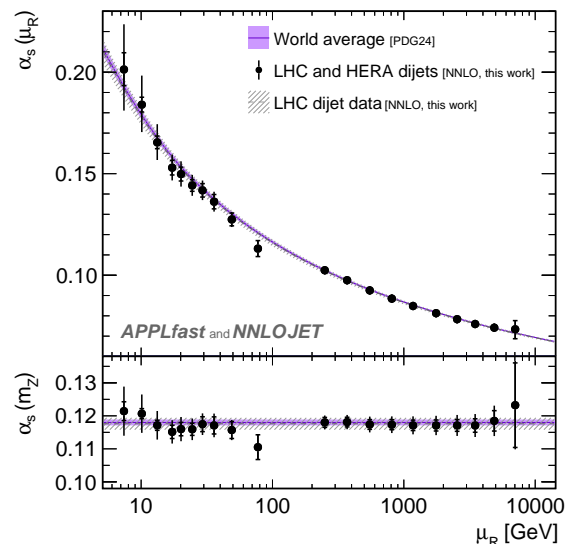

FIG. 2. Running of the strong coupling as a function of the chosen renormalization scale. The inner error bars indicate the (fit,PDF) uncertainty, and the outer error bars the total uncertainty. The upper panel displays the values $\alpha_{\mathrm{s}}(\mu_{\mathrm{R}})$ and the lower panel displays the ratio of the respective $\alpha_{\mathrm{s}}(m_{\mathrm{Z}})$ value to the world average value [6]. The hatched area indicates the value of $\alpha_{\mathrm{s}}(m_{\mathrm{Z}})$ from LHC dijet data and its running as a function of μ_{R}.

We then perform a single fit to all dijet data, where, for each of the individual ranges of m_{jj}, a separate $\alpha_{\mathrm{s}}(m_{\mathrm{Z}})$ value is used for the prediction. In this fit, the assumption of the QCD running enters in each interval only within a very limited range, and in the evolution of the PDFs from μ_0 to μ_{F} (using $\mu_0 = 90$ GeV and $\mu_{\mathrm{F}} = \mu_{\mathrm{R}}$). The technical fit parameter of $\alpha_{\mathrm{s}}(m_{\mathrm{Z}})$ in each interval is evolved to the appropriate scale value $\alpha_{\mathrm{s}}(\mu_{\mathrm{R}})$ as needed for the computation of the NNLO prediction. The advantage of a single fit to determine multiple $\alpha_{\mathrm{s}}(m_{\mathrm{Z}})$ values at a time, in comparison to an alternative approach where each value is determined in a separate fit [23, 27], is that the inference benefits from constraints on the correlated experimental uncertainties, as well as on the PDF uncertainties. In addition, the uncertainties in the resulting $\alpha_{\mathrm{s}}(m_{\mathrm{Z}})$ values have known correlations and these values can therefore be used in further analyses. It has to be noted, that the lowest μ_{R} interval needs to be considered with some care, since these data are below the $2m_b$ threshold, and thus our computations in the five flavor number scheme are at the edge of their validity. However, it is found that these data do not impact other data in the fit, which is also seen from the resulting weak correlations, and thus this result can be neglected also at a later stage. The result at $\mu_{\mathrm{R}} = 7.4$ GeV is therefore reported here for completeness as in previous analyses [23, 40].

The results from this single fit are presented in Table III and the related correlations of the (fit,PDF) uncertainty are listed in Appendix E. The results are com-

pared to the expectation from the QCD RGE in Fig. 2, where in the lower panel the results of the 20 fit parameters for $\alpha_\mathrm{s}(m_\mathrm{Z})$ are displayed, while the upper panel shows the respective values for $\alpha_\mathrm{s}(\mu_\mathrm{R})$. The $\alpha_\mathrm{s}(m_\mathrm{Z})$ values are evolved to the central value of each μ_R interval, illustrating the running of the strong coupling. Overall, excellent agreement with the expectation from the RGE running (when using the world average value for $\alpha_\mathrm{s}(m_\mathrm{Z})$) is observed over the entire range from about 7 GeV up to 7 TeV. At scales of about a few hundred GeV, the size of the experimental and theoretical uncertainties are of similar size (about ±0.0015), while in the TeV regime the experimental uncertainties dominate. In Fig. 3 our results are further compared to α_s extractions from inclusive jet and dijet data by the H1 and ZEUS collaborations at HERA [23, 42], event shape observables at the PETRA or LEP e^+e^- colliders [45–48], a result from a global electroweak fit [6] and measurements of energy–energy correlations in pp collisions by ATLAS at the LHC [27]. Our results exhibit significantly smaller uncertainties and cover a significantly larger range in scale than any previous determination of $\alpha_\mathrm{s}(\mu_\mathrm{R})$.

VI. Summary   We have determined the strong coupling $\alpha_\mathrm{s}(m_\mathrm{Z})$ from dijet data for the first time based on complete NNLO pQCD predictions. Using LHC data collected by the ATLAS and CMS collaborations at center-of-mass energies of 7, 8, and 13 TeV the strong coupling is determined to be

$$\alpha_\mathrm{s}(m_\mathrm{Z}) = 0.1178\,(22)_\mathrm{(tot)}\,,$$

where experimental, PDF, and scale uncertainties are all of similar size. This value is consistent with the world average.

Including dijet cross sections measured in electron–proton collisions at the HERA collider, makes this one of the most comprehensive and precise tests of the QCD renormalization group running of $\alpha_\mathrm{s}(\mu)$ to date. The running is probed by a fit to individual m_jj ranges, and excellent agreement is found with the running predicted by QCD. Through the inclusion of both HERA and LHC data, the behavior of the strong coupling as a function of energy is tested over an unprecedented range, from about 7 GeV to 7 TeV. The presented results significantly improve our knowledge of the strong coupling in the TeV regime compared to previous determinations.

Note added   Recently, the CMS Collaboration has released a determination of α_s and its running in the range 103 GeV $< \mu_\mathrm{R} <$ 1600 GeV using inclusive jet data at the LHC at various $\sqrt{s}$ [49] in addition to HERA DIS data. Their determination make use of NNLO pQCD predictions in the leading-color approximation. Their results are in agreement with ours.
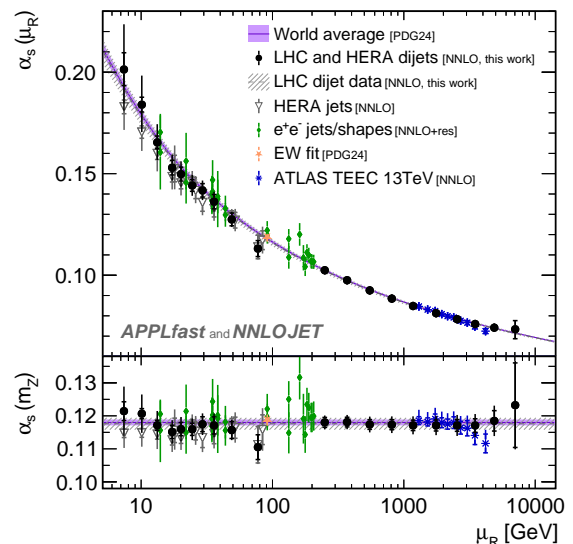
FIG. 3.   Left: Running of the strong coupling as a function of the chosen renormalization scale. The inner error bars indicate the (fit,PDF) uncertainty, and the outer error bars the total uncertainty. The upper panel displays the values $\alpha_\mathrm{s}(\mu_\mathrm{R})$ and the lower panel displays the ratio of the respective $\alpha_\mathrm{s}(m_\mathrm{Z})$ value to the world average value [6]. The hatched area indicates the value of $\alpha_\mathrm{s}(m_\mathrm{Z})$ from LHC dijet data and its running as a function of μ_R. Right: same figure as left, but showing also other data for comparison.

---

[1] H. Fritzsch, M. Gell-Mann, and H. Leutwyler, Phys. Lett. B **47**, 365 (1973).

[2] D. J. Gross and F. Wilczek, Phys. Rev. D **8**, 3633 (1973).

[3] D. J. Gross and F. Wilczek, Phys. Rev. Lett. **30**, 1343 (1973).

[4] H. D. Politzer, Phys. Rev. Lett. **30**, 1346 (1973).

[5] F. Gross *et al.*, Eur. Phys. J. C **83**, 1125 (2023), arXiv:2212.11107.

[6] S. Navas *et al.* (Particle Data Group), Phys. Rev. D **110**, 030001 (2024).

[7] M. Czakon, A. van Hameren, A. Mitov, and R. Poncelet, JHEP **2019**, 262, arXiv:1907.12911.

[8] X. Chen, T. Gehrmann, E. W. N. Glover, A. Huss, and J. Mo, JHEP **2022**, 025, arXiv:2204.10173.

[9] X. Chen, T. Gehrmann, E. W. N. Glover, and J. Mo, JHEP **2022**, 040, arXiv:2208.02115.

[10] G. Aad *et al.* (ATLAS), JHEP **2014**, 059, arXiv:1312.3524.

[11] M. Aaboud *et al.* (ATLAS), JHEP **2018**, 195, arXiv:1711.02692.

[12] S. Chatrchyan *et al.* (CMS), Phys. Rev. D **87**, 112002 (2013), [Erratum: Phys. Rev. D 87, 119902 (2013)], arXiv:1212.6660.

[13] A. M. Sirunyan *et al.* (CMS), Eur. Phys. J. C **77**, 746 (2017), arXiv:1705.02628.

[14] A. Hayrapetyan *et al.* (CMS), Measurement of multidifferential cross sections for dijet production in proton-proton collisions at $\sqrt{s} = 13$ TeV (2023), accepted by: Eur. J. Phys. C, arXiv:2312.16669.

[15] C. Adloff *et al.* (H1), Eur. Phys. J. C **19**, 289 (2001), arXiv:hep-ex/0010054.

[16] F. D. Aaron *et al.* (H1), Eur. Phys. J. C **67**, 1 (2010), arXiv:0911.5678.

[17] H. Abramowicz *et al.* (ZEUS), Eur. Phys. J. C **70**, 965 (2010), arXiv:1010.6167.

[18] V. Andreev *et al.* (H1), Eur. Phys. J. C **75**, 65 (2015), arXiv:1406.4709.

[19] V. Andreev *et al.* (H1), Eur. Phys. J. C **77**, 215 (2017), [Erratum: Eur. Phys. J. C 81, 739 (2021)], arXiv:1611.03421.

[20] Z. Kunszt and D. E. Soper, Phys. Rev. D **46**, 192 (1992).

[21] W. T. Giele, E. W. N. Glover, and J. Yu, Phys. Rev. D **53**, 120 (1996), arXiv:hep-ph/9506442.

[22] G. Dissertori, A. Gehrmann-De Ridder, T. Gehrmann, E. W. N. Glover, G. Heinrich, and H. Stenzel, JHEP **2008**, 040, arXiv:0712.0327.

[23] V. Andreev *et al.* (H1), Eur. Phys. J. C **77**, 791 (2017), [Erratum: Eur. Phys. J. C 81, 738 (2021)], arXiv:1709.07251.

[24] D. Britzger *et al.*, Eur. Phys. J. C **82**, 930 (2022), arXiv:2207.13735.

[25] A. Tumasyan *et al.* (CMS), JHEP **2022**, 142, [Addendum: JHEP 12, 035 (2022)], arXiv:2111.10431.

[26] CMS Collaboration (CMS), The strong coupling constant and its running from inclusive jet production at CMS, http://cds.cern.ch/record/2912634 (2024), CMS-PAS-SMP-24-007.

[27] G. Aad *et al.* (ATLAS), JHEP **2023**, 085, arXiv:2301.09351.

[28] M. Czakon, A. Mitov, and R. Poncelet, Phys. Rev. Lett. **127**, 152001 (2021), [Erratum: Phys. Rev. Lett. 129, 119901, (2022), DOI:10.1103/PhysRevLett.129.119901], arXiv:2106.05331.

[29] M. Alvarez, J. Cantero, M. Czakon, J. Llorente, A. Mitov, and R. Poncelet, JHEP **2023**, 129, arXiv:2301.01086.

[30] M. Cacciari, G. P. Salam, and G. Soyez, JHEP **2008**, 063, arXiv:0802.1189.

[31] J. Currie, A. Gehrmann-De Ridder, T. Gehrmann, N. Glover, A. Huss, and J. Pires, JHEP **2018**, 155, arXiv:1807.03692.

[32] J. Currie, A. Gehrmann-De Ridder, T. Gehrmann, E. W. N. Glover, A. Huss, and J. Pires, Phys. Rev. Lett. **119**, 152001 (2017), arXiv:1705.10271.

[33] A. Gehrmann-De Ridder, T. Gehrmann, E. W. N. Glover, A. Huss, and J. Pires, Phys. Rev. Lett. **123**, 102001 (2019), arXiv:1905.09047.

[34] A. Gehrmann-De Ridder, T. Gehrmann, N. Glover, A. Huss, and T. A. Morgan, PoS **RADCOR2015**, 075 (2016), arXiv:1601.04569.

[35] T. Gehrmann *et al.*, PoS **RADCOR2017**, 074 (2018), arXiv:1801.06415.

[36] D. Britzger, K. Rabbertz, D. Savoiu, G. Sieber, and M. Wobisch, Eur. Phys. J. **C79**, 68 (2019), arXiv:1712.00480.

[37] R. D. Ball *et al.* (PDF4LHC Working Group), J. Phys. G **49**, 080501 (2022), arXiv:2203.05506.

[38] S. Dittmaier, A. Huss, and C. Speckner, JHEP **2012**, 095, arXiv:1210.0438.

[39] Supplementary material: *Consistency study* (cf. section E 1), URL to be provided by publisher, also available as preprint.

[40] D. Britzger *et al.*, Eur. Phys. J. C **79**, 845 (2019), [Erratum: Eur. Phys. J. C 81, 957 (2021)], arXiv:1906.05303.

[41] I. Abt *et al.* (H1, ZEUS), Eur. Phys. J. C **82**, 243 (2022), arXiv:2112.01120.

[42] I. Abt *et al.* (ZEUS), Eur. Phys. J. C **83**, 1082 (2023), arXiv:2309.02889.

[43] J. Currie, T. Gehrmann, and J. Niehues, Phys. Rev. Lett. **117**, 042001 (2016), arXiv:1606.03991.

[44] J. Currie, T. Gehrmann, A. Huss, and J. Niehues, JHEP **2017**, 018, [Erratum: JHEP 12, 042 (2020)], arXiv:1703.05977.

[45] G. Dissertori, A. Gehrmann-De Ridder, T. Gehrmann, E. W. N. Glover, G. Heinrich, G. Luisoni, and H. Stenzel, JHEP **2009**, 036, arXiv:0906.3436.

[46] S. Bethke, S. Kluth, C. Pahl, and J. Schieck (JADE), Eur. Phys. J. C **64**, 351 (2009), arXiv:0810.1389.

[47] J. Schieck, S. Bethke, S. Kluth, C. Pahl, and Z. Trocsanyi (JADE), Eur. Phys. J. C **73**, 2332 (2013), arXiv:1205.3714.

[48] G. Abbiendi *et al.* (OPAL), Eur. Phys. J. C **71**, 1733 (2011), arXiv:1101.1470.

[49] V. Chekhovsky *et al.* (CMS), Determination of the strong coupling and its running from measurements of inclusive jet production (2024), subm. to: Phys. Lett. B, arXiv:2412.16665.

[50] O. V. Tarasov, A. A. Vladimirov, and A. Y. Zharkov, Phys. Lett. B **93**, 429 (1980).

[51] S. A. Larin and J. A. M. Vermaseren, Phys. Lett. B **303**, 334 (1993), arXiv:hep-ph/9302208.

[52] B. Schmidt and M. Steinhauser, Comput. Phys. Commun. **183**, 1845 (2012), arXiv:1201.6149.

[53] A. Vogt, S. Moch, and J. A. M. Vermaseren, Nucl. Phys. B **691**, 129 (2004), arXiv:hep-ph/0404111.

[54] S. Moch, J. A. M. Vermaseren, and A. Vogt, Nucl. Phys. B **688**, 101 (2004), arXiv:hep-ph/0403192.

[55] V. Bertone, S. Carrazza, and J. Rojo, Comput. Phys. Commun. **185**, 1647 (2014), arXiv:1310.1394.

[56] V. Bertone, PoS **DIS2017**, 201 (2018), arXiv:1708.00911.

[57] T. Carli, G. P. Salam, and F. Siegert (Geneva, Switzerland, 2005) p. 110, arXiv:hep-ph/0510324.

[58] T. Carli, D. Clements, A. Cooper-Sarkar, C. Gwenlan, G. P. Salam, F. Siegert, P. Starovoitov, and M. Sutton,

Eur. Phys. J. C **66**, 503 (2010), arXiv:0911.2985.

[59] T. Kluge, K. Rabbertz, and M. Wobisch, Conf. Proc. , 483 (2006), arXiv:hep-ph/0609285.

[60] D. Britzger, K. Rabbertz, F. Stober, and M. Wobisch, Conf. Proc. , 217 (2012), arXiv:1208.3641.

[61] T. Sjöstrand, S. Mrenna, and P. Z. Skands, JHEP **2006**, 026, arXiv:hep-ph/0603175.

[62] T. Sjostrand, S. Mrenna, and P. Z. Skands, Comput. Phys. Commun. **178**, 852 (2008), arXiv:0710.3820.

[63] M. Bahr *et al.*, Eur. Phys. J. C **58**, 639 (2008), arXiv:0803.0883.

[64] J. Bellm *et al.*, Eur. Phys. J. C **76**, 196 (2016), arXiv:1512.01178.

[65] F. James and M. Roos, Comput. Phys. Commun. **10**, 343 (1975).

[66] R. Brun and F. Rademakers, Nucl. Instrum. Meth. **A389**, 81 (1997).

[67] A. Buckley, J. Ferrando, S. Lloyd, K. Nordström, B. Page, M. Rüfenacht, M. Schönherr, and G. Watt, Eur. Phys. J. C **75**, 132 (2015), arXiv:1412.7420.

[68] S. Bailey, T. Cridge, L. A. Harland-Lang, A. D. Martin, and R. S. Thorne, Eur. Phys. J. C **81**, 341 (2021), arXiv:2012.04684.

[69] R. D. Ball *et al.* (NNPDF), Eur. Phys. J. C **77**, 663 (2017), arXiv:1706.00428.

[70] T.-J. Hou *et al.*, Phys. Rev. D **103**, 014013 (2021), arXiv:1912.10053.

[71] S. Alekhin, J. Blümlein, S. Moch, and R. Placakyte, Phys. Rev. D **96**, 014011 (2017), arXiv:1701.05838.

[72] R. D. Ball *et al.* (NNPDF), Eur. Phys. J. C **82**, 428 (2022), arXiv:2109.02653.

[73] H. Abramowicz *et al.* (H1, ZEUS), Eur. Phys. J. C **75**, 580 (2015), arXiv:1506.06042.

Appendix

Appendix A. Theory predictions   The pQCD cross section for the process with two initial-state hadrons is obtained from the factorization formula as the convolution of the PDFs of the incoming protons and the hard scattering cross section

$$\mathrm{d}\sigma = \sum_{a,b} \int \frac{\mathrm{d}x_1}{x_1} \frac{\mathrm{d}x_2}{x_2} f_a(x_1, \mu_{\mathrm{F}}) f_b(x_2, \mu_{\mathrm{F}}) \mathrm{d}\hat{\sigma}_{ab}(\mu_{\mathrm{R}}, \mu_{\mathrm{F}}),$$

where $f_a(x, \mu_{\mathrm{F}})$ denotes the density of the partons of type a in the incoming proton at the factorization scale μ_{F} carrying the longitudinal momentum fraction x. Both contributions are sensitive to the value of α_s, as

$$\mathrm{d}\hat{\sigma}_{ab}(\mu) \equiv \mathrm{d}\hat{\sigma}_{ab}(\mu, \alpha_s(\mu)) \quad \text{and} \quad (A1)$$

$$f_a(x, \mu) \equiv f_a(x, \mu, \alpha_s(\mu)). \quad (A2)$$

The α_{s} dependence in the partonic cross section is explicit through the perturbative expansion, which for dijet production up to NNLO reads

$$\mathrm{d}\hat{\sigma}_{ab}(\alpha_{\mathrm{s}}) = \left(\frac{\alpha_{\mathrm{s}}(\mu)}{2\pi}\right)^2 \mathrm{d}\hat{\sigma}_{ab,\mathrm{LO}} + \left(\frac{\alpha_{\mathrm{s}}(\mu)}{2\pi}\right)^3 \mathrm{d}\hat{\sigma}_{ab,\mathrm{NLO}}$$
$$+ \left(\frac{\alpha_{\mathrm{s}}(\mu)}{2\pi}\right)^4 \mathrm{d}\hat{\sigma}_{ab,\mathrm{NNLO}} + \mathcal{O}(\alpha_{\mathrm{s}}^5(\mu)). \quad (A3)$$

The value of $\alpha_{\mathrm{s}}(\mu)$ is obtained from $\alpha_{\mathrm{s}}(m_{\mathrm{Z}})$ from the renormalization group running in the modified minimal subtraction ($\overline{\mathrm{MS}}$) scheme, i.e. $\alpha_{\mathrm{s}}(\mu) = \alpha_{\mathrm{s},\overline{\mathrm{MS}}}^{(5)}(\mu, \alpha_{\mathrm{s}}(m_{\mathrm{Z}}))$, in three-loop order [50, 51] as implemented in CRun-Dec [52]. The evolution is performed with with $n_f = 5$ active flavors throughout, in particular also beyond the top-quark mass threshold. This is consistent with the perturbative calculation that does not include top-quark effects and thus effectively treats the top quark in the decoupling limit. The evolution of the PDFs with respect

to a scale μ is governed by the DGLAP equations, whose splitting kernels $\mathcal{P}$ depend on $\alpha_{\mathrm{s}}(\mu)$,

$$\mu^2 \frac{\mathrm{d}f}{\mathrm{d}\mu^2} = \mathcal{P}(\alpha_{\mathrm{s}}) \otimes f. \quad (A4)$$

The x-dependence of the PDFs can be fixed at a starting scale μ_0 with value f_{μ_0}, and subsequently evolved to a scale μ using the DGLAP evolution

$$f_a(x, \mu, \alpha_{\mathrm{s}}) = (\Gamma(\mathcal{P}, \mu, \mu_0, \alpha_{\mathrm{s}}) \otimes f_{\mu_0})_a, \quad (A5)$$

where Γ denotes the DGLAP kernels which are evaluated at three-loop order [53, 54] using the program Apfel++ [55, 56]. We set the scale μ_0 of the evolution to $90\,\mathrm{GeV}$ and the x-dependence of $f_{\mu_0,x}$ is taken from PDF4LHC21 [37]. The NNLO cross section is obtained by integrating the dijet parton level predictions (Eq.(A3)) over the bin-dependent kinematic region Ω_i, $\sigma_{\mathrm{NNLO},i} = \int_{\Omega_i} \mathrm{d}\sigma$, using the dijet parton level matrix elements and phase-space integration routines implemented in NNLOJET. Our fit algorithm requires recalculating the predictions for different values of $\alpha_{\mathrm{s}}(m_{\mathrm{Z}})$ and corresponding PDFs. To streamline this, NNLOJET is interfaced with the APPLfast library [24, 40] which integrates the grid tools APPLgrid [57, 58] and fastNLO [59, 60]. The resulting interpolation grids for the dijet data sets typically have sub-permille accuracy. The NNLO prediction is supplemented with additional correction factors to account for non-perturbative effects (NP) and higher-order electroweak (EW) contributions [38], c_{NP} and c_{EW}:

$$\sigma_i = c_{\mathrm{NP},i} \cdot c_{\mathrm{EW},i} \cdot \sigma_{\mathrm{NNLO},i}. \quad (A6)$$

Both correction factors are taken as published by the experimental collaborations [10–14]. A consistent treatment of NP effects across all data sets is desirable but beyond the scope of this article. Hence, different hadronization and parton-shower models are applied, reflecting

variations in the Monte Carlo event generators [61–64] used to derive $c_{\mathrm{NP},i}$. Such variations are considered by the collaborations in the assignment of uncertainties.

Appendix B. Fit algorithm and uncertainties
The objective function used in the fitting algorithm to determine the value of $\alpha_{\mathrm{s}}(m_{\mathrm{Z}})$ is derived from normally distributed relative uncertainties and defined as [18]

$$\chi^2 = \sum_{i,j} \log \frac{\varsigma_i}{\sigma_i} \left(V_{\mathrm{exp}} + V_{\mathrm{NP}} + V_{\mathrm{NNLOstat}} + V_{\mathrm{PDF}}\right)^{-1}_{ij} \log \frac{\varsigma_j}{\sigma_j},$$

where the double-sum runs over all data points, ς_i denotes the measured cross section, σ_i denotes the theory prediction. The χ^2 is minimized using TMinuit's Migrad algorithm [65, 66]. The covariance matrices V_{exp}, V_{NP}, V_{NNLOstat}, and V_{PDF} represent the relative experimental, NP, NNLO statistical, and PDF uncertainties, respectively. The experimental uncertainties are reported by the experimental collaborations and account for many systematic sources as well as statistical components including correlations from unfolding. Correlations between the experimental uncertainties of individual data sets are not provided and hence are assumed to be uncorrelated, which is certainly correct for the statistical components. A recent report from CMS [26] using inclusive jet data at different $\sqrt{s}$ indicates that the dominating uncertainty from jet energy calibration and resolution may be considered as uncorrelated between such data sets, supporting that the omission of correlations is justified. The non-perturbative correction uncertainties (cf. Sec. A) are considered to have a bin-to-bin correlation of 0.5. This approximated correlation model accounts for varying multiple model parameters, different models, and potential statistical components. The NNLO statistical uncertainties originate from the Monte Carlo integration in NNLOJET and are typically at the percent level or below. The PDF uncertainties are obtained from the respective PDF set in the LHAPDF format [67], and evaluated at μ_0. By considering them as a covariance matrix in χ^2, the PDF uncertainties are further constrained by the jet data. The PDFs carry further uncertainties due to differing theoretical assumptions, data selections, and inference methods imposed by the PDF fitting groups. In the PDF4LHC21 PDF set, however, such differences are already included in the uncertainty representation [37] and represent differences between the MSHT [68], NNPDF3.1 [69] and CT18 [70] PDFs. Dedicated fits using these different PDF sets confirm that the PDF uncertainty indeed covers such differences. Results when using yet different PDFs, such as ABMP [71], NNPDF4.0 [72], or HERAPDF2.0 [73], are typically found to be well within 2σ of the PDF uncertainty.

Appendix C. Fits using CMS 13 TeV triple-differential data
The CMS Collaboration reported dijet cross sections at $\sqrt{s} = 13\,\mathrm{TeV}$ also in triple-differential variants as a function of y^*, y_{b}, and m_{jj} or

$\langle p_{\mathrm{T}} \rangle_{1,2}$ [14]. Besides observables and different binnings, the analyzed data and experimental methods are equivalent in these three variants, and therefore these data sets cannot be used in a fit together because of their experimental correlations. This section discusses the triple-differential measurement $\frac{\mathrm{d}^3\sigma}{\mathrm{d}m_{\mathrm{jj}}\mathrm{d}y^*\mathrm{d}y_{\mathrm{b}}}$ for a determination of $\alpha_{\mathrm{s}}(m_{\mathrm{Z}})$ instead of their double-differential variant (cf. Tab. I) When restricting the data to $y^* < 2.0$ and $y_{\mathrm{b}} < 1.0$, similar to the fits in Sec. II, the fit to these data results in a value of χ^2/n_{dof} of 1.23 for 113 data points and provides $\alpha_{\mathrm{s}}(m_{\mathrm{Z}}) = 0.1181\,(20)_{(\mathrm{fit},\mathrm{PDF})}\,(1)_{(\mu_0)}\,(15)_{(\mu_{\mathrm{R}},\mu_{\mathrm{F}})}$. Using the triple-differential data as an alternative to the double-differential variant in the combined fit, the value

$$\alpha_{\mathrm{s}}(m_{\mathrm{Z}}) = 0.1172\,(14)_{(\mathrm{fit},\mathrm{PDF})}\,(0)_{(\mu_0)}\,(14)_{(\mu_{\mathrm{R}},\mu_{\mathrm{F}})}$$

is derived with χ^2/n_{dof} of 0.99. The result is in good agreement with that obtained when using the double-differential data. For the main analysis presented in this letter, the double-differential CMS data is chosen rather than the triple-differential cross sections, as the sensitivity to the PDF parameters is lower, and the double-differential data reaches higher values of m_{jj}, while the sensitivity of the data to $\alpha_{\mathrm{s}}(m_{\mathrm{Z}})$ is similar.

Appendix D. Including HERA dijet data
We extend our analysis by further including data for inclusive dijet production in neutral-current deep-inelastic scattering (NC DIS) reported by the H1 [15, 16, 18, 19] and ZEUS [17] collaborations, together with complete NNLO pQCD predictions [40, 43, 44]. These data have already been used for α_{s} determinations at NNLO accuracy [23, 41, 42], and thus, the method and data selection from H1 [23] is closely followed: four data sets at $\sqrt{s} = 300$ and $320\,\mathrm{GeV}$ at lower or higher photon virtualities Q^2 being considered, and the fit methodology differing only in the choices for the PDF and μ_0. In addition, data from the ZEUS collaboration recorded at $\sqrt{s} = 320\,\mathrm{GeV}$ and for $Q^2 > 125\,\mathrm{GeV}^2$ are also included, similar to Refs. [41, 42]. All five data sets, summarized in Tab. IV, employ the k_{t} jet algorithm with $R = 1.0$ and represent double-differential cross sections as a function of Q^2 and $\langle p_{\mathrm{T}} \rangle_{1,2}$. The ZEUS data are restricted

Data set	$\sqrt{s}$ [GeV]	Cuts
H1 300 GeV high-Q^2 [15]	300	–
H1 HERA-I low-Q^2 [16]	320	$\mu > 2m_b$
H1 HERA-II low-Q^2 [19]	320	$\mu > 2m_b$
H1 HERA-II high-Q^2 [18]	320	–
ZEUS HERA-I+II high-Q^2 [17]	320	$\langle p_{\mathrm{T}} \rangle_{1,2} > 15\,\mathrm{GeV}$

TABLE IV. Summary of the HERA data sets for dijet production with the k_{t} jet algorithm with jet size parameter $R = 1.0$.

to $\langle p_{\mathrm{T}} \rangle_{1,2} > 15\,\mathrm{GeV}$ to exclude infrared sensitive data points [44]. At lower Q^2, data points with a typical scale smaller than twice the bottom quark mass ($\mu < 2m_b$) are excluded in the nominal fit, since the predictions

$\mu_{\rm R}$ [GeV]	Correlations																			
7.4	–	56	29	21	19	22	15	17	16	12	2	1	-1	-2	-3	-3	-3	-3	-1	0
10.1	56	–	65	50	49	50	37	38	36	23	9	8	5	2	0	-2	-3	-3	-2	0
13.3	29	65	–	58	52	54	40	45	39	23	11	11	9	7	5	2	1	0	0	1
17.2	21	50	58	–	48	52	39	44	41	24	9	9	8	7	5	3	2	1	1	1
20.1	19	49	52	48	–	52	39	38	41	24	9	9	9	8	7	5	4	2	1	1
24.5	22	50	54	52	52	–	55	49	53	36	10	11	11	10	9	7	5	3	2	1
29.3	15	37	40	39	39	55	–	41	44	33	6	8	9	10	9	8	7	5	3	1
36.0	17	38	45	44	38	49	41	–	39	28	5	6	8	8	8	7	5	3	1	
49.0	16	36	39	41	41	53	44	39	–	31	4	5	6	7	8	7	6	5	3	1
77.5	12	23	23	24	24	36	33	28	31	–	1	2	2	3	4	4	3	2	1	
250	2	9	11	9	9	10	6	5	4	0	–	90	87	83	78	71	64	54	36	9
370	1	8	11	9	9	11	8	6	5	1	90	–	95	91	87	80	72	61	40	10
550	-1	5	9	8	9	11	9	8	6	2	87	95	–	97	93	88	80	67	45	11
810	-2	2	7	7	8	10	10	8	7	2	83	91	97	–	97	93	86	74	49	12
1175	-3	0	5	5	7	9	9	8	8	3	78	87	93	97	–	97	92	80	55	14
1760	-3	-2	2	3	5	7	8	8	7	4	71	80	88	93	97	–	96	87	62	17
2545	-3	-3	1	2	4	5	7	7	6	4	64	72	80	86	92	96	–	92	70	21
3490	-3	-3	0	1	2	3	5	5	5	3	54	61	67	74	80	87	92	–	78	27
4880	-1	-2	0	1	1	2	3	3	3	2	36	40	45	49	55	62	70	78	–	30
7040	0	0	1	1	1	1	1	1	1	1	9	10	11	12	14	17	21	27	30	–

TABLE V. Correlations of the (fit,PDF) uncertainty from the fit of 20 $\alpha_{\rm s}(m_{\rm Z})$ parameters to HERA and LHC dijet data.

are performed with $n_f = 5$ [23]. The correlations between data sets are described in Refs. [23, 41]. The scales are identified with $\mu_{\rm R}^2 = \mu_{\rm F}^2 = Q^2 + \langle p_{\rm T} \rangle_{1,2}^2$. From fits to individual data sets, consistent results are obtained for $\chi^2/n_{\rm dof}$ and $\alpha_{\rm s}(m_{\rm Z})$ for the H1 data as in Ref. [23]. For the ZEUS data a value of $\chi^2/n_{\rm dof} = 11.8/15$ is obtained with $\alpha_{\rm s}(m_{\rm Z}) = 0.1164\,(33)_{\rm (fit,PDF)}\,(20)_{(\mu_{\rm R},\mu_{\rm F})}$. A fit to all HERA dijet data result in a value $\alpha_{\rm s}(m_{\rm Z}) = 0.1177\,(14)_{\rm (fit,PDF)}\,(1)_{(\mu_0)}\,(33)_{(\mu_{\rm R},\mu_{\rm F})}$ with $\chi^2/n_{\rm dof} = 92.8/118$. As expected, these results are very similar to those reported from H1 data alone [23], as the ZEUS dijet data add only modestly to the sensitivity. These results represent the first determination of $\alpha_{\rm s}(m_{\rm Z})$ at NNLO using only DIS dijet production, including data from H1 and ZEUS. The value of $\alpha_{\rm s}(m_{\rm Z})$ as determined in a single fit to HERA and LHC dijet data taken together was reported in Table II (cf. Sec. D). This analysis benefits from theory predictions for dijet production at NNLO and from independent, and thus fully uncorrelated, experimental setups. When the triple-differential data from CMS at 13 TeV are used instead of the double-differential variants in that fit, a value of $\alpha_{\rm s}(m_{\rm Z})$ of

$$0.1177\,(10)_{\rm (fit,PDF)}\,(0)_{(\mu_0)}\,(27)_{(\mu_{\rm R},\mu_{\rm F})}$$

is obtained with $\chi^2/n_{\rm dof}$ of 0.95 for 520 individual data points. This result is in good agreement with that obtained using the double-differential data instead.

Appendix E. Resulting correlations   The resulting correlations of the (fit,PDF) uncertainty in the combined fit of 20 parameters to the HERA and LHC dijet data are listed in Table V. These correlations originate from the combined determination of 20 fit parameters and from correlated uncertainties between individual cross section values. In the region where HERA or LHC data are important, $\mu_{\rm R}$ smaller or larger 100 GeV respectively, the correlations originate predominantly from correlated experimental systematic uncertainties. Hence, correlations are found to be positive. Correlations between low and high scales, respectively between HERA and LHC data, originate from PDF uncertainties.

The additional (μ_0) and $(\mu_{\rm R},\mu_{\rm F})$ uncertainties are fully correlated.

Supplementary material

1. Consistency study

Before determining the value of $\alpha_s(m_Z)$ from dijet cross section measurements, we perform a study to investigate the agreement between the NNLO pQCD predictions and the data, and to test the self-consistency of the individual data sets, as well as the consistency of multiple data sets together.

a. Individual data sets

Determinations of α_s are performed for individual y^*, y_b, y_{max} bins of the individual data sets. Each double-differential data sets has five or six y^* (y_b, y_{max}) ranges, and these are studied separately in the following. For the triple-differential CMS 8 TeV cross sections we study the six (y^*,y_b)-bins separately. For the triple-differential CMS 13 TeV data, three studies are performed for individual y^*, y_b, or y_{max} ranges. We consider the PDF sets PDF4LHC21 [37], CT18 [70], MSHT [68], NNPDF3.1 [69], NNPDF4.0 [72], ABMP [71], and HERAPDF2.0 [73]. In addition, we study fits, where the PDF uncertainties are not considerd in the χ^2 calculus (denoted as Excl. $\delta_{(PDF)}$). The resulting values of χ^2/n_{dof} of these fits with a variety of PDF sets are displayed in FIG. 4.
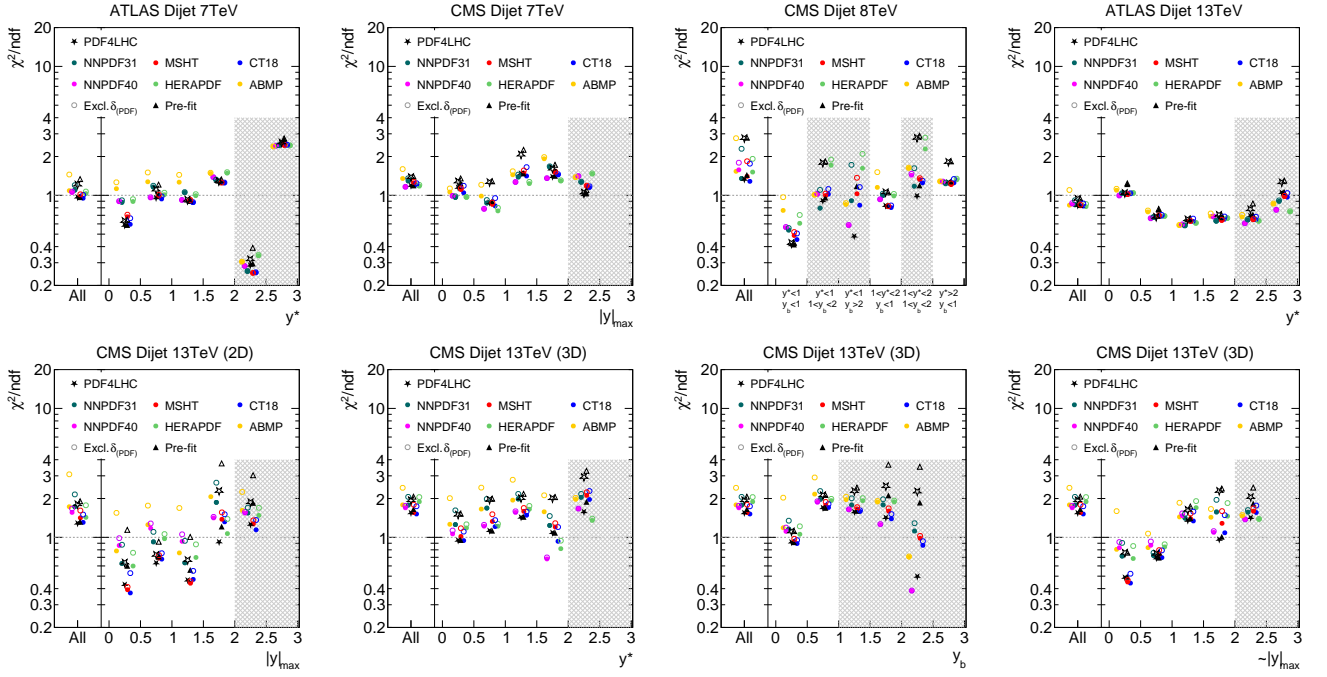

FIG. 4. Post-fit χ^2/n_{dof} values of $\alpha_s(m_Z)$-fits to individual y^* or y_b-ranges of each data set, and values from fits to entire single data sets (denoted as *All*). The top row shows dijet cross sections from ATLAS and CMS at 7 TeV, CMS at 8 TeV, and ATLAS at 13 TeV. The bottom row shows the χ^2/n_{dof} values for the double-differential data from CMS at 13 TeV (left), and three studies of the triple-differential CMS 13 TeV data for individual y^*, y_b, or y_{max} ranges. The color coding indicates different PDF sets, as specified in the Panel. The colored markers are vertically displaced for better visibility. The open markers indicate post-fit values, where V_{PDF} is not included in the χ^2-calculus, for each of the PDF set studied. The black triangle indicates the pre-fit value of the nominal NNLO pQCD predictions, when using the PDF4LHC21 PDF set. The shaded area indicates ranges, which are not included in the nominal combined fits (for the CMS 13 TeV triple-differential data, there is some ambiguity due to the second y cut, y^* or y_b, respectively).

It is observed that the pre-fits yield reasonable χ^2 values, indicating an initial good agreement between the NNLO predictions and the data. Significant exceptions are only observed for very large values of y^*, y_b, or y_{max}, which may be related to the increased PDF dependence in these kinematic regions, and either poorly determined PDFs or too tight PDF uncertainities. It is further observed that the post-fit values of χ^2/n_{dof} yield reasonable values ranging from 0.29 to 2.5, while most of the values are around unity, i.e. in the range between 0.6 to 1.3. The χ^2/n_{dof} values for

the different PDF sets are reasonably consistent. The values for ABMP and HERAPDF2.0 are slightly higher, which is expected, since these PDFs include few or no data from the LHC experiments. The PDF4LHC21 PDF set shows good agreement with the data in all fits, and this PDF set has often one of the smallest χ^2/n_{dof} values of all PDF variants, which supports the choice of PDF4LHC21 for our main result. In several fits, the χ^2/n_{dof} values without PDF uncertainty are somewhat larger than those with PDF uncertainties included, which indicates the importance of the PDF uncertainty in these bins. The χ^2/n_{dof} values of the fits to all data of a single data set (All) also yield reasonable values with χ^2/n_{dof} value ranging from 0.8 to 1.6. However, for some data sets, these χ^2/n_{dof} values are somewhat larger than the ones obtained for individual y ranges. This may indicate some slight tension in these data and originate from the assumptions of the correlation model of the data systematic uncertainties, or from PDFs.

In conclusion, we observe, that the NNLO predictions provide an overall good description of the data and are suitable for an unbiased determination of $\alpha_s(m_Z)$. For our nominal fits, we impose cuts on $y^* < 2.0$ and $y_b < 1.0$ to reduce the PDF sensitivity and reduce some moderate tensions within certain data sets.

b. Multiple data sets analysed together

To assess the consistency between the individual data sets, α_s fits are performed considering data points from all data sets. Since the CMS 13 TeV data are provided in both double- and triple-differential forms, but only one of the two data sets can be included in this combined study due to their statistical correlations, we perform the study twice, once for each data set.

The various data sets are provided for distinct y^* or $|y|_{\mathrm{max}}$ ranges, and we define three intervals in the following: $0 \leq y^* < 1$, $1 \leq y^* < 2$, $y^* \geq 2$ (the $|y|_{\mathrm{max}}$-ranges from Ref. [12] are interpreted as y^* for this particular study).
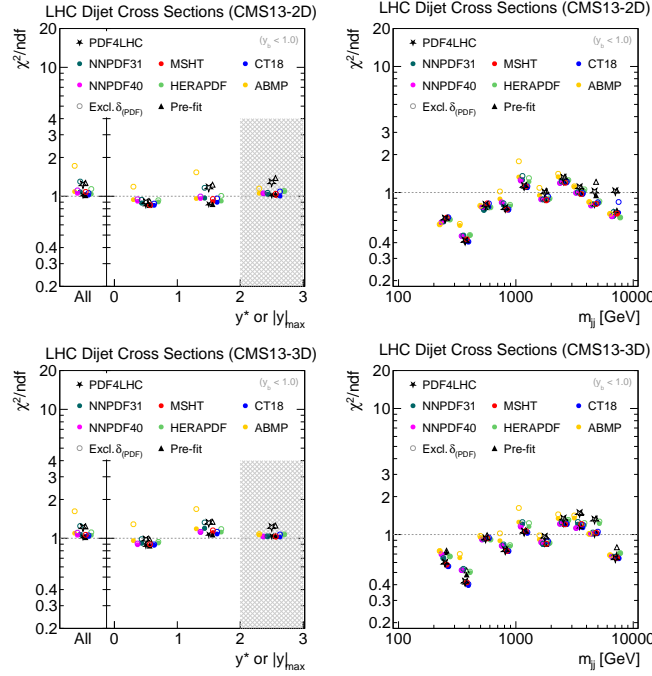

FIG. 5. Left: Post-fit values of χ^2/n_{dof} of α_s-fits in three distinct y^*-ranges ($0 \leq y^* < 1$, $1 \leq y^* < 2$, $y^* \geq 2$). More details, see Fig. 4. Right: Post-fit values of χ^2/n_{dof} of α_s-fits in nine distinct m_{jj}-ranges. Excellent consistency of the four data sets, and the data and NNLO predictions is observed. The leftmost entries show the χ^2/n_{dof} values of the nominal combined fit to all dijet data.

The resulting χ^2/n_{dof} values are displayed in Fig. 5 (left) and excellent χ^2/n_{dof} values around unity are obtained for all three y^* ranges and for different PDF sets. It is also observed that including PDF uncertainties in χ^2 alters the χ^2/n_{dof} values only slightly, which indicates an excellent agreement of the PDFs with the data, as well as small PDF uncertainties. However, a fit to all three y^* ranges at a time yields a somewhat increased χ^2/n_{dof} value and thus indicating a slight tension between all data. In order to avoid a possible bias from that, and to reduce further the PDF dependence, we drop the data with $y^* > 2$ (or $y_{\mathrm{max}} > 2$, respectively) in the nominal fit. This restriction

removes jets in the outer rapidity regions, where the endcap calorimeters are important and tracking detectors are not available.

In order to assess the consistency of the data across different m_{jj} regions, nine adjacent ranges between $200\,\mathrm{GeV}$ and $9\,\mathrm{TeV}$ are defined in m_{jj}, with an approximately equidistant width in $\log(m_{jj})$, similar to the data intervals. For the data of Ref. [13], which are measured as a function of $p_{\mathrm{T,avg}}$, the m_{jj}-interval is sampled with the NNLO calculation, and the average m_{jj} values are found to range from 218 to $5396\,\mathrm{GeV}$. Nine fits to the individual m_{jj} ranges are performed and the resulting χ^2/n_{dof} values are displayed in FIG. 5 (right). Altogether, reasonable values of χ^2/n_{dof} are obtained. At lower values of m_{jj}, the values are below unity, whereas at $m_{jj} \approx 2.5\,\mathrm{TeV}$ they are somewhat larger with values of about 1.2. The inclusion of the PDF uncertainties in the χ^2 has only a limited impact on the resulting χ^2/n_{dof} values, indicating little sensitivity to the PDF parameters and good agreement with PDFs, given the imposed cuts on y^* and y_b ($ys < 2$ and $y_b < 1$).

c. HERA dijet data

In this section, we present a study of the consistency of the dijet data from H1 and ZEUS, using the NNLO pQCD predictions. Similar studies have previosuly been performed by the H1 Collaboration for the H1 data sets [23], and for a combination of ZEUS dijet data and selected H1 data sets in Ref. [41]. Nonetheless, we perform a study similar to those performed for the LHC data, considering all H1 dijet data sets [15, 16, 18, 19] along with the dijet data from ZEUS [17]. The χ^2/n_{dof} value for each data set and multiple PDF sets are displayed in FIG. 6.
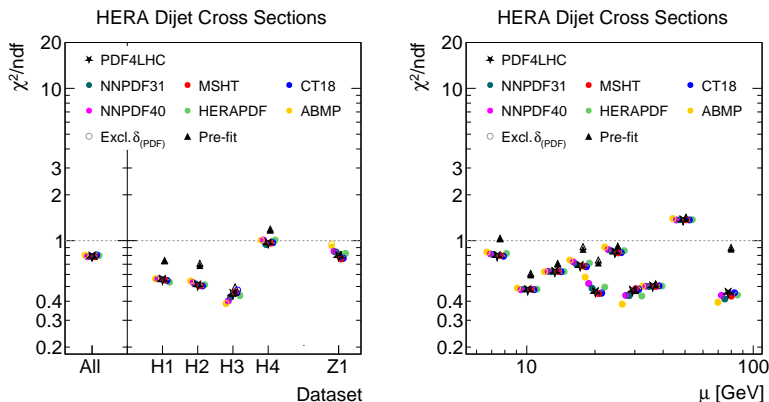

FIG. 6. Left: Post-fit values of χ^2/n_{dof} of α_s fits for five dijet data sets from HERA. Four data sets from H1 for center-of-mass energies and Q^2 ranges are studied, and labeled as H1 [15], H2 [16], H3 [19] and H4 [18], and the data set from ZEUS is labeled Z1 [17]. The combined fit to all HERA data is labelled as 'All'. Right: Post-fit values of χ^2/n_{dof} of α_s-fits to all five HERA dijet data sets in ten distinct μ ranges. See FIG. 4 for more details.

The χ^2/n_{dof} values for the H1 data sets are very similar to those reported in Ref. [23]. Similarly, the χ^2/n_{dof} value for the ZEUS data confirms the good agreement between the data and the NNLO predictions, as previously reported [17]. The combined fit to all HERA data results in an excellent χ^2/n_{dof} with a value of 0.79, thus confirming excellent consistency between the different data sets and of the data with the NNLO predictions. Different PDF sets have only little impact on the χ^2/n_{dof} values, which may be explained by the strong impact of the HERA inclusive DIS data on PDFs. Subsequently, the data are grouped into ten μ intervals with $\mu = Q^2 + \langle p_{\mathrm{T}} \rangle^2_{1,2}$ [23]. The resulting χ^2/n_{dof} values for these fits are also very good. Although some moderate flucutations in χ^2/n_{dof} are observed across different μ intervals, no systematic deterioration is evident.

This study confirms that the HERA dijet data can be used for an unbiased determination of the running of α_s together with the NNLO predictions across their full range. However, we exclude the lowest μ interval because it falls below twice the mass of the bottom quark. Our calculations are performed for five massless quark flavors and are therefore not strictly valid for these data, although they still provide an excellent description of them.